

Effect of Surface Pore Structure of Nerve Guide Conduit on Peripheral Nerve Regeneration

Se Heang Oh, PhD,^{1,*} Jin Rae Kim, MS,^{1,*} Gu Birm Kwon, MS,²
Uk Namgung, PhD,² Kyu Sang Song, MD,³ and Jin Ho Lee, PhD¹

Polycaprolactone (PCL)/Pluronic F127 nerve guide conduits (NGCs) with different surface pore structures (nano-porous inner surface vs. micro-porous inner surface) but similar physical and chemical properties were fabricated by rolling the opposite side of asymmetrically porous PCL/F127 membranes. The effect of the pore structure on peripheral nerve regeneration through the NGCs was investigated using a sciatic nerve defect model of rats. The nerve fibers and tissues were shown to have regenerated along the longitudinal direction through the NGC with a nano-porous inner surface (Nanopore NGC), while they grew toward the porous wall of the NGC with a micro-porous inner surface (Micropore NGC) and, thus, their growth was restricted when compared with the Nanopore NGC, as investigated by immunohistochemical evaluations (by fluorescence microscopy with anti-neurofilament staining and Hoechst staining for growth pattern of nerve fibers), histological evaluations (by light microscopy with Meyer's modified trichrome staining and Toluidine blue staining and transmission electron microscopy for the regeneration of axon and myelin sheath), and FluoroGold retrograde tracing (for reconnection between proximal and distal stumps). The effect of nerve growth factor (NGF) immobilized on the pore surfaces of the NGCs on nerve regeneration was not so significant when compared with NGCs not containing immobilized NGF. The NGC system with different surface pore structures but the same chemical/physical properties seems to be a good tool that is used for elucidating the surface pore effect of NGCs on nerve regeneration.

Introduction

PERIPHERAL NERVES FUNCTION as communication paths between the brain and muscle/organ/skin, and injury to these nerves leads to the severe loss of sensory or motor functions.¹ Although the understanding of nerve regeneration and the development of surgical techniques are rapidly growing, sufficient restoration of damaged nerves still remains a big challenge.^{2,3} Recently, artificial nerve guide conduit (NGC) to bridge the gap between severed peripheral nerve stumps has been demonstrated to be a promising strategy for the treatment of damaged nerves. NGCs can provide a favorable micro-environment for nerve regeneration and properly guide the axonal sprouting from the proximal stump to the distal stump to reinnervate its original target.⁴⁻⁶ There are essential requirements for desirable NGCs, including mechanical properties that provide space for nerve regeneration and surgical facility.⁷⁻⁹ It is well known that surface electric charges¹⁰ and bioactive molecules¹¹⁻¹⁴ can affect nerve regeneration through NGCs. The

morphology of the NGCs was also shown to be an important factor for nerve regeneration.¹⁵⁻¹⁷ The earlier NGCs had dense and impermeable walls, which prevented the invasion of nerve regeneration inhibitors. Although this morphology was demonstrated to provide an appropriate environment for axonal outgrowth inside the lumen, it was reported that the impermeable NGCs lead to suppressed nerve regeneration due to hindered nutrient supply. To overcome this drawback, many researchers have tried to fabricate porous (nano-, micro-, or more widely open porous) NGCs for improved permeability.^{3,18-24} Although the effect of pores in the NGCs on nerve regeneration has been evaluated, it still remains controversial. It was demonstrated that porous NGCs enhance nerve regeneration,^{5,16,23,25-31} possibly due to vascularization into the pore structure,^{23,31} high permeability for nutrients/oxygen,^{26,31} fast drainage of nerve wound exudates,^{27,29} or neural cell alignment^{16,30} in porous NGCs. It was also shown that the connective stroma fill porous NGCs, which prevents nerve regeneration through the NGC.^{15,32-34} The strong adhesion between regenerated neural tissues and

¹Department of Advanced Materials, Hannam University, Daejeon, South Korea.

²Department of Oriental Medicine, Daejeon University, Daejeon, South Korea.

³Department of Pathology, School of Medicine, Chungnam National University, Daejeon, South Korea.

*These two authors contributed equally to this work.

the porous surface of NGC was also shown to negatively impact nerve regeneration.¹⁵ These inconsistencies may be due to the use of NGCs with different pore sizes, pore structures, or permeability as well as different physical/chemical properties. It is clear that neural tissue formation in the NGC is affected by the surface pore structure; however, nerve regeneration may be dependent on the complex combination of many parameters, and the exact factors that are most relevant to nerve regeneration are not yet fully understood. Thus, if NGCs with similar permeability and physical/chemical properties but different surface pores can be prepared, the effect of pore structure on nerve regeneration can be more clearly assessed.

The main aim of this study was to develop NGCs with different surface pores but similar membrane properties and to systematically investigate the effect of surface pores (nano- or micro-size pores) on nerve regeneration through NGCs. To achieve this goal, an asymmetrically porous polycaprolactone (PCL)/Pluronic F127 membrane (nano- and micro-pores on both surfaces) was fabricated using a novel immersion precipitation method.³⁵ The PCL/F127 NGCs with different surface pore structures (nano-porous inner surface vs. micro-porous inner surface) were simply fabricated by rolling the opposite side of asymmetrically porous membranes (Fig. 1). The nerve growth factor (NGF), as a stimulation source that enhances peripheral nerve regeneration, was also immobilized onto the pore surfaces of the PCL/F127 NGCs through the specific interaction between the Pluronic F127 and heparin (hydrogen bonding) and the subsequent interaction between heparin and NGF (ionic interaction).³⁶ The PCL/F127 NGCs with different surface pore structures were implanted into rats (a sciatic nerve defect model), and the nerve regeneration behaviors through the NGCs were compared. Figure 2 demonstrates the schematic diagrams of NGCs with different surface pore structures.

Materials and Methods

Materials

PCL (Mw 80,000; Aldrich), Pluronic F127 (Mw 12,500; BASF), and tetraglycol (glycofurol; Sigma) were used to prepare NGCs. Pluronic F127 was used as a hydrophilic additive to PCL, and tetraglycol was used as a nontoxic cosolvent for PCL and Pluronic F127. NGF (recombinant rat NGF) was selected as a stimulation source to enhance the peripheral nerve regeneration and was purchased from R&D Systems. All other chemicals were of an analytical grade and were used as received. Ultrapure grade water (>18 mΩ) was purified using a Milli-Q purification system.

Fabrication of NGCs

NGCs with different surface pore structures (nano-porous inner surface vs. micro-porous inner surface) were prepared using asymmetrically porous PCL/F127 membranes with selective permeability and hydrophilicity (nano- and micro-pores on both surfaces). The asymmetrically porous PCL/F127 membranes were fabricated by the immersion precipitation method.³⁵ For this, PCL pellets were dissolved in tetraglycol at 90°C (12 wt.%), and Pluronic F127 powder was added in the PCL solution with dif-

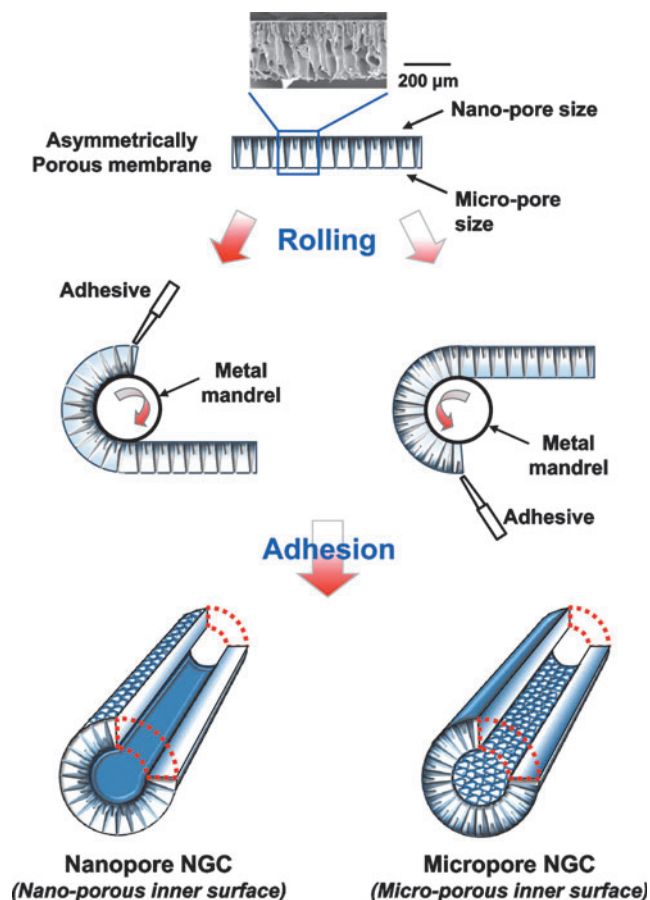


FIG. 1. Schematic diagrams showing the process used to fabricate the NGCs with different surface pore structures (nano-porous inner surface vs. micro-porous inner surface) by rolling the opposite side of the asymmetrically porous PCL/Pluronic F127 membranes. NGC, nerve guide conduits; PCL, polycaprolactone. Color images available online at www.liebertpub.com/tec

ferent Pluronic F127 compositions (0–10 wt.%, PCL base). The hot PCL/F127 mixture solution was cast in a mold (50×50×0.4 mm) and directly immersed in excess water for 1 h at room temperature. The asymmetrically porous PCL/F127 membrane was obtained after washing in excess water to remove residual solvent and vacuum drying. The tube-shaped NGCs with different pore structures were simply fabricated by rolling the opposite side of the prepared asymmetrically porous membranes (see Fig. 1). The membranes were rolled into a tube using a metal mandrel (diameter, 1.5 mm), and the overlapped end of the membrane was adhered tightly using a tissue adhesive, *N*-butyl-2-cyanoacrylate (Histoacryl®; B. Braun). The prepared NGCs had a ~1.5 mm inner diameter, ~12 mm length, and ~0.4 mm wall thickness.

The morphologies of the PCL/F127 membranes and NGCs were investigated using a scanning electron microscope (SEM, JSM-6335F; JEOL). The average pore sizes on the membrane surfaces were determined based on the SEM images using an image analysis program (i-solution, IMT). The inner diameter and wall thickness of the NGC were measured directly from the SEM pictures.

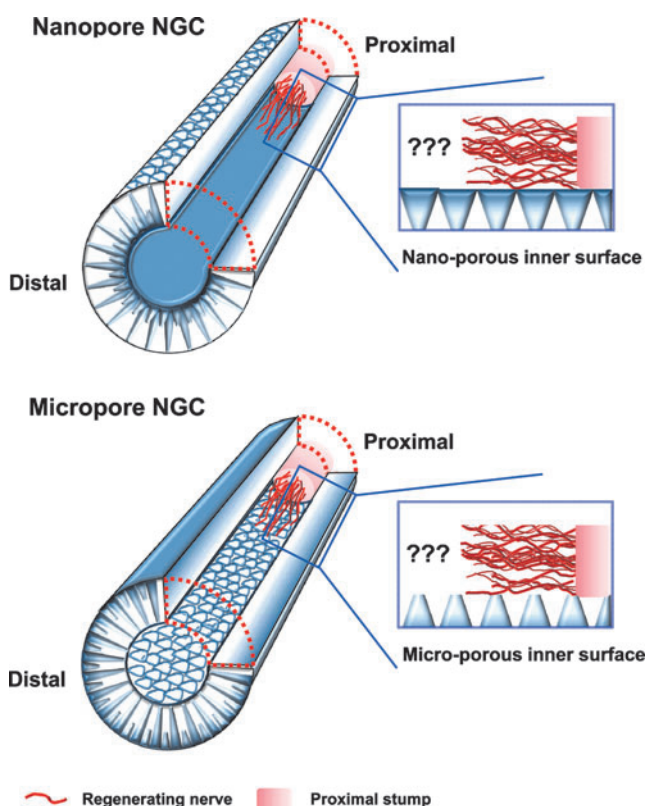


FIG. 2. Schematic diagrams showing the Nanopore NGC (with nano-porous inner surface) and Micropore NGC (with micro-porous inner surface), and their nerve regeneration potential through the NGCs. Color images available online at www.liebertpub.com/tec

NGF immobilization and release profile

NGF, which was used to enhance peripheral nerve regeneration, was incorporated onto the pore surfaces of the PCL/F127 NGCs via heparin immobilization. In order to immobilize heparin, the NGCs with different Pluronic F127 compositions were soaked in a heparin solution (1 mg/mL [in 2 wt.% NaCl solution]) at 4°C for 3 h. The heparin-immobilized NGCs were rinsed with 2 wt.% NaCl solution and water successively, and then freeze dried. The amount of heparin immobilized on the NGCs was determined using the Toluidine blue assay.³⁷ In order to incorporate the NGF onto the heparin-immobilized PCL/F127 NGCs, the NGCs were soaked in an NGF solution (500 ng/mL) at room temperature for 6 h. The NGF-immobilized NGCs were washed thrice with phosphate-buffered saline (PBS; pH ~7.4), and the amount of immobilized NGF was quantified using a direct enzyme-linked immunosorbent assay (ELISA) technique,³⁸ according to the standard ELISA procedures provided in the kit (Duoset®, R&D systems). The NGF-adsorbed PCL and PCL/F127 NGCs without heparin immobilization were also prepared using the same procedure just described to evaluate the effect of heparin immobilized onto the pore surfaces of the NGCs on the NGF binding and release profile. To investigate the release profile, the NGF-immobilized (or adsorbed) NGCs were incubated in 1 mL PBS supplemented with 1% bovine serum albumin (BSA) at 37°C for up to 35 days under mild shaking (~50 rpm). At preset time intervals, the whole medium was collected and replaced with

fresh PBS. The amount of NGF released in the collected medium was determined using an ELISA kit.

Implantation of NGCs

Sprague-Dawley (SD) rats (weight, ~250 g) were used to evaluate the peripheral nerve regeneration behavior through the PCL/F127 NGCs (with or without NGF immobilization) with different pore structures (nano-porous inner surface vs. micro-porous inner surface). A total of 48 rats were used for the analyses. The animals were divided into four groups (12 rats/group): NGC with a nano-porous inner surface (Nanopore NGC), NGF-immobilized NGC with a nano-porous inner surface (Nanopore NGC/NGF), NGC with a micro-porous inner surface (Micropore NGC), and NGF-immobilized NGC with a micro-porous inner surface (Micropore NGC/NGF). Each group was divided into four sub-groups for the different analyses (three rats/sub-group): analyses for immunohistochemical evaluation, toluidine blue staining and transmission electron microscope (TEM) observations, histological evaluation, and FluoroGold (FG) retrograde tracing (refer to the evaluation methods below). The animal study was approved by the Animal Care Committee of the Hannam University in Korea, and all procedures were performed according to the appropriate guidelines. Anesthesia was administered through an intramuscular injection of tiletamine/zolazepam (10 mg/kg, Zoletil 50®, Virbac Laboratories) and 2% xylazine hydrochloride (2 mg/kg, Rumpun®, Byely). The sciatic nerve on the left side was exposed, and a 10 mm segment of the nerve was removed from the mid-thigh level. NGCs with 12 mm in length were connected between the proximal and distal stumps with two sutures [7-0 polydioxanone (PDS); Ethicon] at each junction. After implantation, the muscle incision was closed using a 5-0 chromic catgut suture (Ethicon), and the skin was closed with a 5-0 nylon suture (Ethicon).

Immunohistochemical evaluation

To investigate the nerve fiber growth pattern from the proximal to distal stumps through the NGCs, the animals were euthanized at 4 weeks postimplantation, and the NGCs, including regenerated nerve inside, were carefully dissected. The specimens were frozen immediately at -80°C and cut into longitudinal sections with a thickness of 20 μm. The specimens were mounted on positively charged slides (Fisher Scientific Co.) and fixed with 4% paraformaldehyde and 4% sucrose in PBS for 45 min. The specimens for anti-neurofilament staining were then permeabilized with 0.5% nonidet P-40 (Fluka) in PBS for 40 min at room temperature and blocked with 2.5% horse serum and 2.5% BSA in PBS containing 10% Triton X-100 (PBST) for 12 h at 4°C. To visualize the growth pattern of nerve fibers, the sections were subjected to immunofluorescence staining with primary antibodies against NF-200 (neurofilament-200, mouse monoclonal, 1:200; Sigma) and S100β (rabbit polyclonal, 1:400; Dako), respectively, and detected by incubation with fluorescein-labeled goat anti-mouse immunoglobulin G (IgG) (for NF-200; 1:400; Invitrogen) or rhodamine-labeled goat anti-rabbit IgG (for S100β; 1:400; Invitrogen) secondary antibodies in 2.5% horse serum and 2.5% BSA in PBST for 1.5 h in a dark room. For cellular nuclei, the sections mounted on the slides were stained with 2.5 μg/mL of Hoechst 33258

(bis-benzimide; Invitrogen) for 10 min before the final wash with 0.1% PBST. The stained sections were cover-slipped with an aqueous mounting medium (Blomeda). The sections were observed under a fluorescent microscope (Model BX51; Olympus). The control sections were treated with secondary antibody alone, which usually did not produce any visible fluorescent signals. If the nonspecific signals were high, the data were not used.

Histological evaluation

For histological analysis, Meyer's modified trichrome staining and Toluidine blue staining were conducted. For Meyer's modified trichrome staining, the dissected NGCs were fixed with 4% paraformaldehyde and 4% sucrose in PBS, then embedded in paraffin wax, and cut into 5 μ m transverse sections (3 mm position from the proximal end of NGC for the initial growth pattern view of nerve fibers). The specimens were stained with Meyer hematoxylin solution (Sigma) and Gomori's trichrome staining solution, including fast green FCF, chromotrope 2R, phosphotungstic acid, and glacial acetic acid (Sigma). The specimens were rinsed in 0.6% acetic acid solution, dehydrated, mounted, and examined by light microscopy. For Toluidine blue staining, the regenerated nerve specimens were fixed with 2.5% glutaraldehyde in 0.1 M PBS for 2 h and postfixed in 1% osmium tetroxide for 1.5 h. The samples were then dehydrated in a graded ethanol series and embedded in an Epon 812 resin (Polysciences). The mid-portions of the specimens were cut into thin cross-sections with a thickness of 1 μ m using an ultra-microtome (MT-XL; RMC, Inc.), stained with Toluidine blue, and observed by light microscopy. The diameter of the myelinated axon, thickness of the myelin sheath, and total area of neural tissue in the regenerated nerves were estimated using an image analysis program (i-solution). To observe more detailed axon and myelin sheath regeneration through the NGCs, the specimens were also cut into ultrathin sections with a thickness of 50–60 nm. The sections were stained with lead citrate and uranyl acetate, and then examined by a TEM (Model H-7650; Hitachi).

To evaluate the atrophy of muscle caused by the malfunction of the sciatic nerve, the gastrocnemius muscles of the NGC-implanted side (left side) were harvested, and the specimens were cut from the mid-belly of the gastrocnemius muscle and fixed with 4% formaldehyde in PBS. The specimens were embedded in paraffin wax and cut into 5 μ m transverse sections. These sections were subjected to Masson's trichrome staining for the observation by a light microscope. The diameter of the muscle fibers and collagen fiber area in the muscle sections were estimated based on the light microscope images ($\times 200$ magnification) using an image analysis program (i-solution).

FG retrograde tracing

Retrograde tracing with FG was performed to examine the reconnection between proximal and distal stumps. For this, 10 μ L of 5% FG in saline (Invitrogen) was injected into the sciatic nerve trunk that was positioned 10 mm from the distal end of the NGC at 4 weeks after NGC implantation. One week after FG injection, the animals were euthanized, the spinal cord was carefully exposed, and dorsal root ganglions (DRGs) at lumbar 5 and 6 level of the spinal cord were dis-

sected. The specimens were frozen immediately at -80°C and cut into transverse sections with a thickness of 20 μ m to investigate the FG fluorescence of DRGs. The sections were mounted on positively charged slides and examined under a fluorescent microscope.

Statistical analysis

The data obtained from each NGC group were averaged and expressed as the mean \pm standard deviation. Student's *t*-test was used to determine the significance of the differences between each NGC group. The differences were considered statistically significant at $p < 0.05$.

Results and Discussion

Morphology of NGCs

Porous NGCs with different surface pore structures were fabricated by rolling the opposite side of asymmetrically porous PCL/F127 membranes (see Fig. 1), and the effect of surface pore structure (nano- or micro-size pores) on nerve regeneration through NGCs was investigated. Figure 3 shows the gross appearance and surface morphology of the PCL/F127 (5 wt.%) NGCs with different pore structures (nano-porous inner surface vs. micro-porous inner surface). The asymmetrically porous membrane was produced by placing the PCL/F127 mixture solution in tetraglycol in contact with water (nonsolvent for PCL) during the membrane fabrication process.³⁵ The top surface (water contact side) of the membrane contained nano-size pores (~ 100 nm), whereas the opposite surface (mold contact side) contained micro-size pores (~ 200 μ m), and both sides were connected by an asymmetric column-shape pore structure. The nano-size pores on the membrane could effectively prevent the

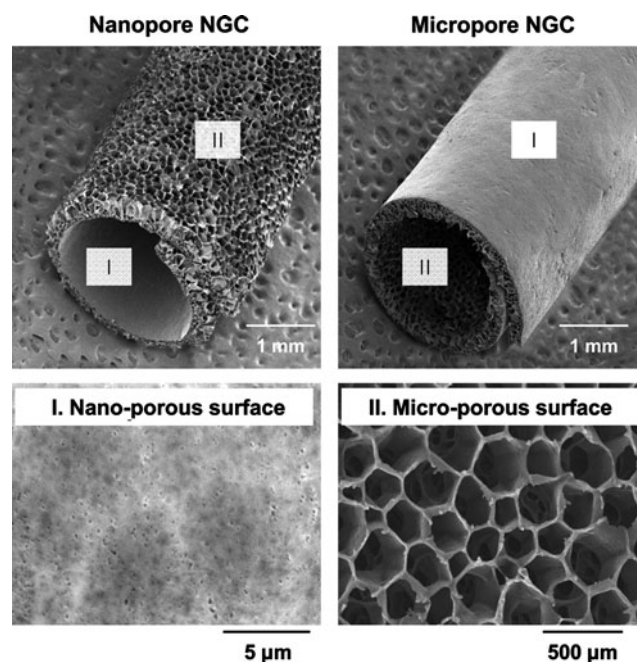


FIG. 3. Scanning electron microscope photographs showing the gross appearance and surface morphology of the Nanopore NGC and Micropore NGC prepared by rolling the opposite side of the asymmetrically porous PCL/F127 (5 wt.%) membranes.

infiltration of fibrous tissues (several 10 μm sizes), while allowing for the permeation of nutrients (much smaller sizes, 4–12 nm) (i.e., selective permeability).^{31,35,39} The unique morphology of the PCL/F127 membrane was due to the creation of a polymer concentration gradient along the height direction in the polymer solution during the polymer precipitation in water.⁴⁰ The PCL/F127 membranes containing 0, 1, 3, and 5 wt.% Pluronic F127 had an asymmetric column-shape porous structure; however, the membrane containing 10 wt.% Pluronic F127 had a collapsed pore structure (data not shown). Therefore, the asymmetrically porous PCL/F127 membranes with Pluronic F127 compositions up to 5 wt.% were used for further studies. The NGCs with different pore structures (Nanopore and Micropore NGCs) could be easily prepared by rolling the opposite side of the asymmetrically porous membranes without structure distortion.

NGF immobilization and release profile

NGF, which has been recognized to promote peripheral nerve regeneration and prevent nerve cell loss after a peripheral nerve injury,^{41,42} was incorporated onto the porous NGCs with a different pore structure. To incorporate NGF on the PCL/F127 NGCs, heparin was first immobilized on the NGC via intermolecular hydrogen bonding between the Pluronic F127 (ether oxygen) exposed on the pore surfaces of the NGC and heparin (carboxylic acid).⁴³ The amount of heparin immobilized on the pore surfaces of the NGCs increased significantly with an increase in the Pluronic F127 composition (PCL, $1.28 \pm 0.17 \mu\text{g}/\text{NGC}$; PCL/F127 [1 wt.%], $2.35 \pm 0.07 \mu\text{g}/\text{NGC}$; PCL/F127 [3 wt.%], $4.39 \pm 1.03 \mu\text{g}/\text{NGC}$; PCL/F127 [5 wt.%], $6.28 \pm 0.13 \mu\text{g}/\text{NGC}$), indicating that the Pluronic F127 chains were sufficiently exposed on the pore surfaces of the NGCs and effectively interacted with heparin. Based on these experiments, 5 wt.% addition of Pluronic F127 into the PCL matrix was shown to be optimal for PCL/F127 NGC fabrication, in terms of their morphology and heparin immobilization. Thus, the PCL/F127 (5 wt.%) NGC was utilized for NGF immobilization. The amounts of heparin immobilized on the pore surfaces were not different between the Nanopore and Micropore NGCs.

NGF immobilization on the NGCs was quantitatively assessed by ELISA. The loading amounts of NGF adsorbed (PCL and PCL/F127) or immobilized (PCL/F127/heparin) on the NGCs were estimated to be $101.35 \pm 23.63 \text{ ng}$, $115.89 \pm 21.66 \text{ ng}$, and $323.96 \pm 64.52 \text{ ng}$, respectively (Fig. 4A). The heparin-immobilized NGC (PCL/F127/heparin) had a significantly higher loading amount of NGF than the NGCs without heparin (PCL and PCL/F127), which was likely due to the ionic interactions between the heparin (O-sulfate and N-sulfate groups) and growth factor (certain lysine and arginine residues).⁴⁴ Figure 4B shows the time-dependent release profile of NGF from the NGCs. The heparin-immobilized PCL/F127 NGC showed a moderate burst release of NGF at the initial stage (for 3 days), and then, the NGF was continuously released by up to $\sim 80\%$ of the initial loading ($\sim 260 \text{ ng}$) over 35 days. The rapid desorption of nonspecifically bound NGF on the PCL/F127/heparin NGC may have led to this initial burst.⁴⁵ The sustained release of NGF most likely occurred due to the slow dissociation of ionic bonds between surface-immobilized heparin and NGF on the NGC. On the other hand, the NGCs without heparin

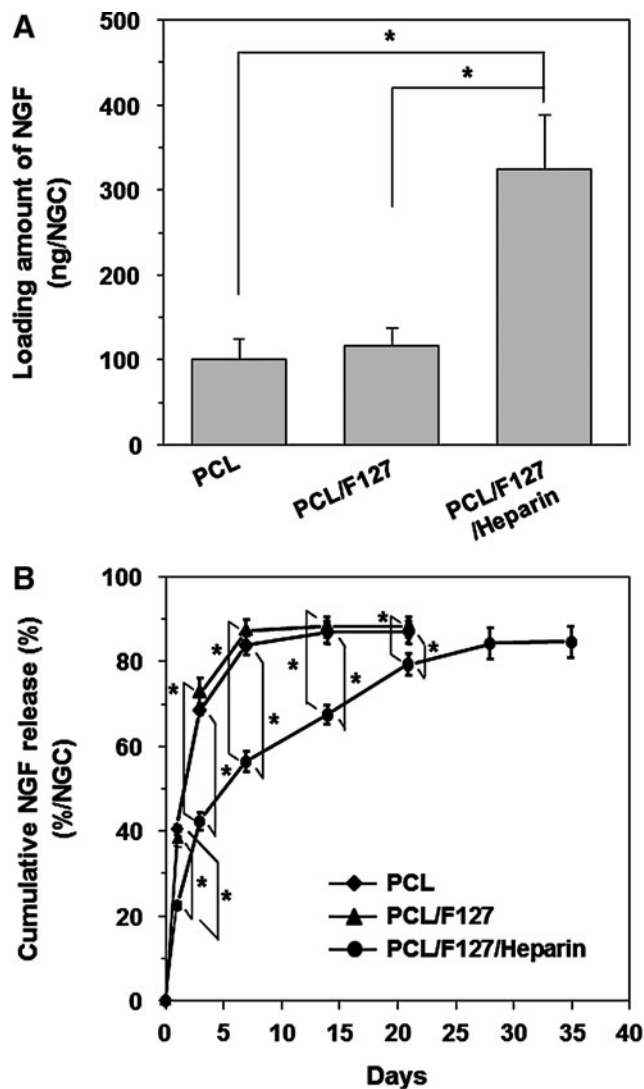


FIG. 4. (A) Loading and (B) cumulative released amounts of NGF from the PCL, PCL/F127, and PCL/F127/heparin NGCs ($n=3$; $*p<0.05$). The heparin-immobilized NGC (PCL/F127/heparin) had a significantly higher loading amount of NGF than the NGCs without immobilized heparin (PCL and PCL/F127), which was probably due to the ionic interactions between heparin and NGF molecules. The PCL/F127/heparin NGC showed a moderate burst release of NGF at the initial stage (for 3 days), and then, the NGF was continuously released over 35 days. NGF, nerve growth factor.

immobilization showed a much faster initial burst over the initial 3 days, and almost all of the NGF loaded on the NGCs was released within 7 days. The NGF loading amount and release profile were not also significantly different between the Nanopore NGC/NGF and Micropore NGC/NGF. The sustained release of NGF from the NGCs with selective permeability and hydrophilicity may accelerate the peripheral nerve regeneration rate, and, thus, can provide a more effective environment for peripheral nerve regeneration.

Evaluations for nerve fiber growth pattern

SD rat (sciatic nerve defect model) was used to evaluate the effect of pore structure (Nanopore and Micropore NGCs)

on peripheral nerve regeneration through the NGCs. Four weeks after NGC implantation, the nerve fiber growth pattern through the NGC was observed by anti-neurofilament staining (NF-200 for axon; S100 β for myelin), Hoechst staining (for cell nuclei), and Meyer's modified trichrome staining (for myelinated axon). Figure 5 shows the longitudinal sections of the regenerated nerve through NGCs from the anti-neurofilament staining (NF-200). For the Nanopore NGC and NGC/NGF groups, the axon grew along the longitudinal direction of the NGC and re-bridged between the proximal and distal stumps at 4 weeks (Fig. 5A, B). The Nanopore NGC/NGF showed higher axon density (fibrous green color) than the Nanopore NGC without NGF, indicating faster nerve regeneration (Fig. 5B). This may be due to the continuous release of NGF from the conduit, which can enhance nerve regeneration.^{41,42} On the other hand, the Micropore NGC and NGC/NGF groups showed much slower axonal growth and regenerating nerve fibers (Fig. 5C, D), even when NGF was continuously released from the conduit (Fig. 5D). In our previous study, we also demonstrated that the Nanopore NGC allowed much faster nerve regeneration than the nonporous silicone tube.³¹ Interestingly, in the Nanopore NGC/NGF, the migrating cells derived from the proximal stump (e.g., Schwann cells, fibroblasts, etc.; blue color from the Hoechst staining) (Fig. 6A) were predominantly positioned at the central region in the NGC without attachment on the conduit wall surface and were aligned

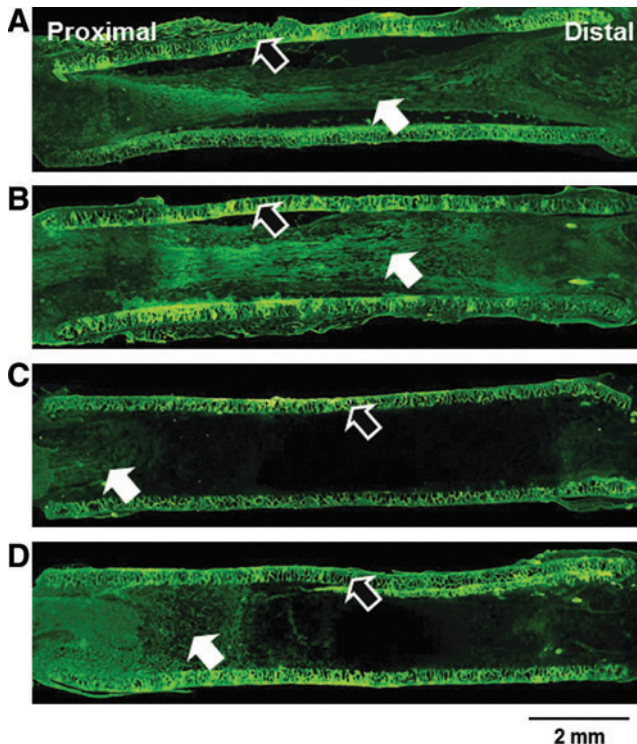


FIG. 5. Longitudinal sections of the regenerated nerve through (A) Nanopore NGC, (B) Nanopore NGC/NGF, (C) Micropore NGC, and (D) Micropore NGC/NGF (4 weeks after implantation; anti-neurofilament staining [NF-200], $\times 4$; white arrow, regenerated nerve; black arrow, NGC). The Nanopore NGCs showed faster axonal growth than the Micropore NGCs, regardless of the presence of NGF. Color images available online at www.liebertpub.com/tec

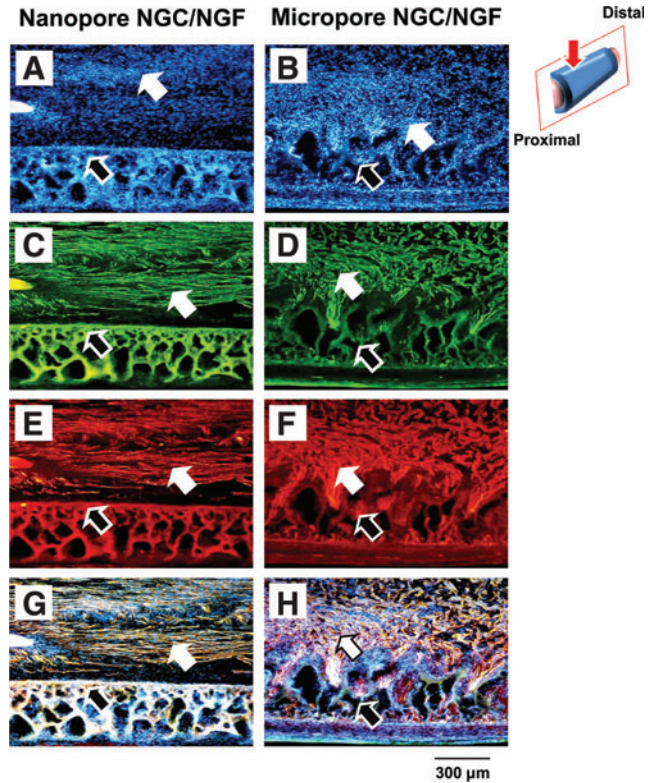


FIG. 6. Longitudinal sections of the regenerated nerve fibers through the Nanopore NGC/NGF and Micropore NGC/NGF. (A, B) Hoechst staining; (C, D) NF-200 staining; (E, F) S100 β staining; and (G, H) their merged images (4 weeks after implantation; $\times 100$; white arrow, regenerated nerve fiber; black arrow, NGC; red arrow, observation position). For the Nanopore NGC/NGF, the migrating cells were predominantly positioned at the central region in the NGC without attachment on the conduit wall surface. The regenerating nerve fibers were arranged along the longitudinal direction of the conduit. In contrast, for the Micropore NGC/NGF, the cells were scattered without any arrangement, and the regenerated nerve fibers had infiltrated into the porous wall of the conduit. Color images available online at www.liebertpub.com/tec

toward the longitudinal direction, and, thus, the regenerating nerve fibers [green (axon) from the NF-200 staining (Fig. 6C); red (myelin) from the S100 β staining (Fig. 6E)] were oriented along the longitudinal direction of the conduit. In addition, they were not attached on the conduit wall, probably due to its smooth (nano-size pores) character. Based on the merged images of the cell distribution and nerve fiber growth in the NGC (Fig. 6G), we believe that the cells include many Schwann cells which can guide axonal sprouting.^{46,47} However, in the Micropore NGC/NGF, the cells were scattered throughout the NGC without any arrangement, a large number of cells had infiltrated into the porous wall (Fig. 6B), and the regenerated nerve fibers also grew toward the porous wall of the conduit (Fig. 6D, F, and H), which restricted nerve regeneration along the longitudinal direction between proximal and distal stumps. From the Meyer's modified trichrome staining using transverse sections of the Nanopore NGC/NGF, axon fiber spots with a relatively high density (by the perpendicular section of axonal fibers [red color]) were observed in the regenerated nerve tissues as well as

blood vessels (Fig. 7), indicating that axonal sprouting toward the distal stump and angiogenesis occurred during the nerve regeneration process. From the transverse section view of the Micropore NGC/NGF, oblique-shaped axon fibers (red color) created by the slanting section were observed in the regenerated nerve tissues (many of them inside the porous wall of the conduit), indicating that axonal sprouting toward the porous wall (along the transverse direction) occurred during nerve regeneration. These phenomena may be explained by the alignment direction of fibrin matrices (or strands) and Schwann cells at the initial nerve repair stage for regenerating axons. During endogenous nerve regeneration, plasma-derived precursor proteins create an oriented fibrin matrix along the longitudinal direction between the proximal and distal stumps, and the Schwann cells migrate following the fibrin matrix.^{46–49} Then, the Schwann cells proliferate, form the band of Büngner, and guide axonal regrowth.^{46,50–53} It is well known that the morphology of the fibrin matrix created at the initial stage and the distribution of Schwann cells within NGC govern the final morphology of the regenerated nerve fibers.^{54,55} Although we did not investigate the morphology of the fibrin matrix within the

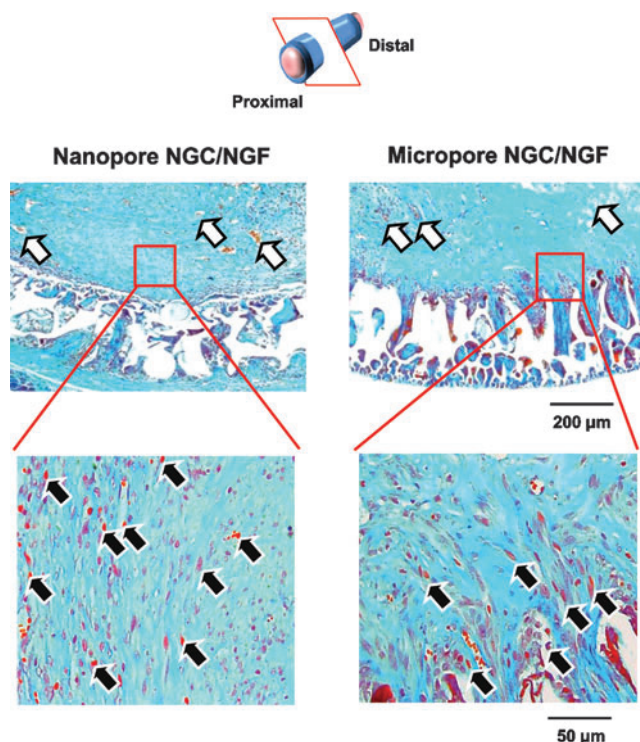


FIG. 7. Transverse sections of the regenerated nerve fibers in the NGCs (4 weeks after implantation; 3 mm position from the proximal end; Meyer's trichrome staining; $\times 100$ and $\times 400$; white arrow, blood vessel; black arrow, regenerated axon). For the Nanopore NGC/NGF, axon fiber spots created by the perpendicular section of axonal fibers (red color) were observed in the regenerated nerve tissues, indicating that axonal sprouting toward the distal stump occurred. However, for the Micropore NGC/NGF, oblique-shaped axon fibers created by the slanting section of axonal fibers were detected (many of them, inside the porous wall of the conduit), suggesting that the axonal sprouting toward the porous wall of the conduit occurred. Color images available online at www.liebertpub.com/tec

NGCs, we could hypothesize that the Nanopore NGC allows for the production of oriented fibrin strands, where the Micropore NGC did not, based on the cell distributions in the NGC (i.e., the oriented cell distribution in the NGC indicates the well-aligned fibrin matrix) (refer to Fig. 6A, B). The NGF-immobilized NGCs (Nanopore NGC/NGF and Micropore NGC/NGF) showed more dense nerve fibers than the NGCs without NGF (Nanopore NGC and Micropore NGC); however, their nerve fiber growth patterns were not highly different (not shown the data of the NGC groups without NGF). Many previous studies have reported that NGCs with a smooth surface^{46,48,54,56–58} provide an appropriate environment for an aligned fibrin matrix and, thus, allow for the formation of a neural structure in the NGCs. More recently, it was also demonstrated that the oriented topography in the NGC can enhance cellular alignment, and, therefore, accelerate nerve regeneration.^{59–62}

Evaluations for nerve regeneration

At 4 weeks postimplantation, the nerve regeneration behavior of the NGCs in terms of axon diameter, myelin sheath thickness, and area occupied by neural tissue (axon and myelin sheath) was compared between the Nanopore NGC (with and without NGF) and Micropore NGC (with and without NGF). The regenerated nerve in the NGCs was observed at the middle section under a light microscope after Toluidine blue staining and by a TEM to provide a more detailed view of myelinated axons in the NGCs (Fig. 8). The

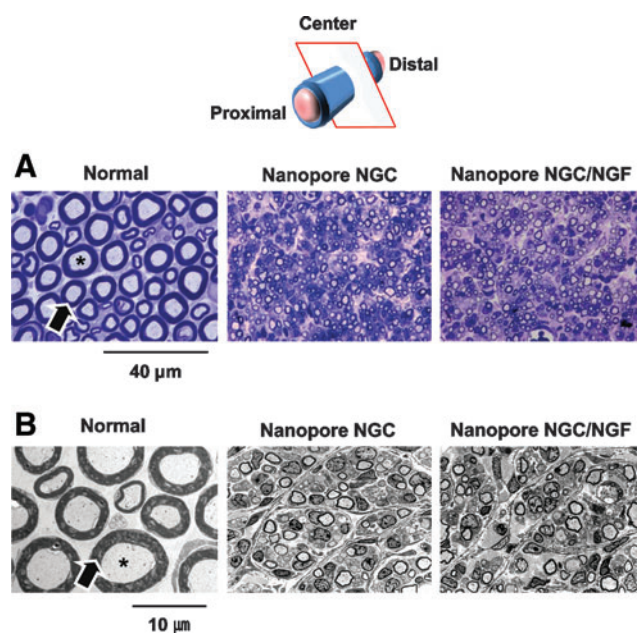


FIG. 8. (A) Light micrographs of semi-thin sections (Toluidine blue staining; $\times 1000$) and (B) Transmission electron microscope images of ultrathin sections ($\times 3000$) showing myelinated axons at the mid-portion of the Nanopore NGC and NGC/NGF 4 weeks after implantation (asterisk, axon; arrow, myelin). The Nanopore NGCs allowed for the nerve regeneration within the conduit. The Nanopore NGC/NGF showed a slightly (but not significantly) larger axon diameter and a thicker myelin sheath than the Nanopore NGC without NGF. Color images available online at www.liebertpub.com/tec

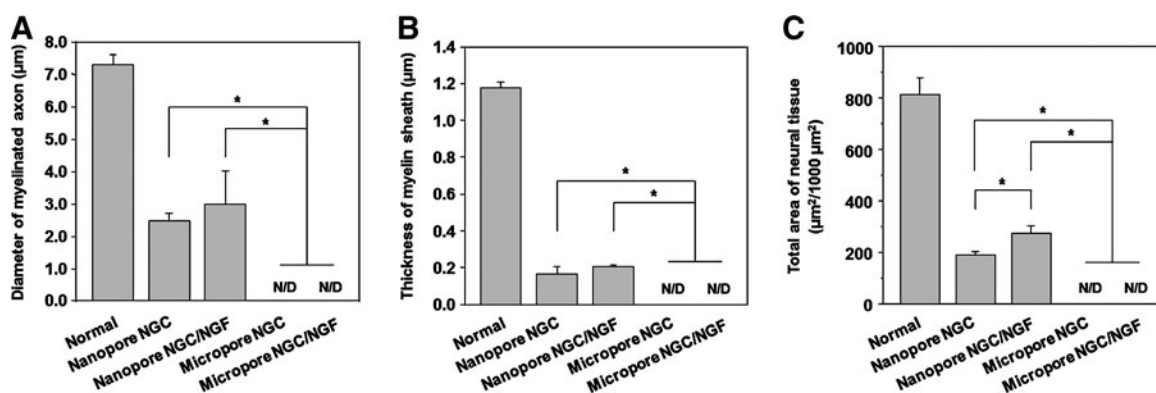


FIG. 9. Comparison of (A) the diameter of the myelinated axon, (B) thickness of myelin sheath, and (C) area occupied by neural tissue in the NGC at the middle section 4 weeks after implantation ($n=3$; $*p < 0.05$; N/D, no detection). The Nanopore NGCs show significantly faster nerve regeneration compared with the Micropore NGCs.

Nanopore NGCs allowed for nerve regeneration within the NGC at the middle section (5 mm position from the proximal end) 4 weeks after implantation. The Nanopore NGC/NGF showed a slightly larger axon diameter and a thicker myelin sheath than the Nanopore NGC without NGF. However, any regenerated nerves within the Micropore NGCs at the same position was not detected, even for the NGF-immobilized NGC (data, not shown), indicating that the nerve regeneration through the NGC with micro-porous inner surface was impeded. Figure 9 compares the diameter of the myelinated axon, thickness of myelin sheath, and area occupied by neural tissue in the Nanopore NGCs with those of normal rat nerve. The diameter of the axon and thickness of the myelin sheath in the Nanopore NGC/NGF were 41% and 17%, respectively, relative to the normal nerve (axon diameter, $2.97 \pm 1.03 \mu\text{m}$ and myelin sheath thickness, $0.20 \pm 0.01 \mu\text{m}$). The Nanopore NGC without NGF had a smaller axon diameter and a myelin sheath thickness (axon diameter, $2.46 \pm 0.24 \mu\text{m}$ and myelin sheath thickness, $0.16 \pm 0.04 \mu\text{m}$), which was $\sim 20\%$ lesser than those of the NGF-immobilized NGC group. The Nanopore NGC/NGF had a larger neural tissue area than the Nanopore NGC without NGF (Normal, $815.38 \pm 62.94 \mu\text{m}^2$; Nanopore NGC, $191.47 \pm 11.67 \mu\text{m}^2$; Nanopore NGC/NGF, $273.07 \pm 31.48 \mu\text{m}^2$).

To determine whether the reconnection between proximal and distal stumps occurred through the NGCs or not, FG retrograde tracing was performed. FG-labeled neuron cells (gold color) were observed in the DRGs of the Nanopore NGC (with and without NGF)-implanted groups at 1 week after FG injection (Fig. 10). The Nanopore NGC/NGF group contained more FG-labeled neuron cells compared with the Nanopore NGC group, which indicated that the greater nerve fibers connecting the defect stumps were present. However, FG-labeled cells in the DRGs were not detected in the Micropore NGC groups, even for the NGF-immobilized NGC group.

To evaluate the extent of reinnervation of target muscle, the diameter of muscle fibers and collagen fiber area in the gastrocnemius muscle, which are governed by nerve signals transmitted through the sciatic nerve, were compared between the Nanopore and Micropore NGCs (with and without NGF). All experiment groups showed diminished muscle fibers and increased collagen fibers when compared with the normal group, indicating atrophy of muscle caused by the

severe nerve defect (Fig. 11). The muscle immediately starts to atrophy, which leads to the hypoplasia of muscle fibers and the hyperplasia of collagen fibers, when sciatic nerve injury occurs. However, the Nanopore NGCs showed significantly faster recovery from the muscle atrophy (thicker diameter of muscle fiber and smaller collagen fiber area) due to reinnervation of muscle than the Micropore NGCs, regardless of NGF immobilization. The Nanopore NGC/NGF seemed to provide a better environment for muscle reinnervation than the Nanopore NGC, probably due to the continuous release of NGF from the NGC. These results showed that the Nanopore NGCs allow for much better nerve regeneration than the Micropore NGCs and immobilization of NGF on the NGCs accelerated the nerve regeneration, which are in agreement with the results shown in

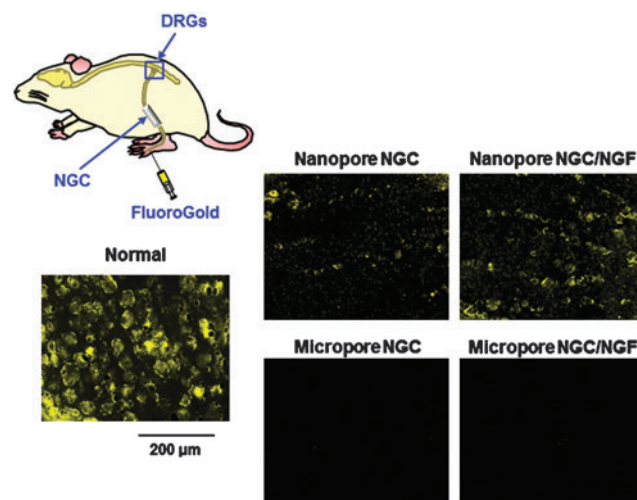


FIG. 10. Fluorescent micrographs following FluoroGold (FG) retrograde tracing in the DRGs of the NGC-implanted group 1 week after FG injection ($\times 100$). The Nanopore NGC/NGF group contained more FG-labeled neuron cells compared with the Nanopore NGC group, indicating that a greater number of nerve fibers connecting the defect stumps were present. However, FG-labeled cells in the DRGs were not detected in the Micropore NGC groups, even for the NGF-immobilized NGC group. DRG, dorsal root ganglions. Color images available online at www.liebertpub.com/tec

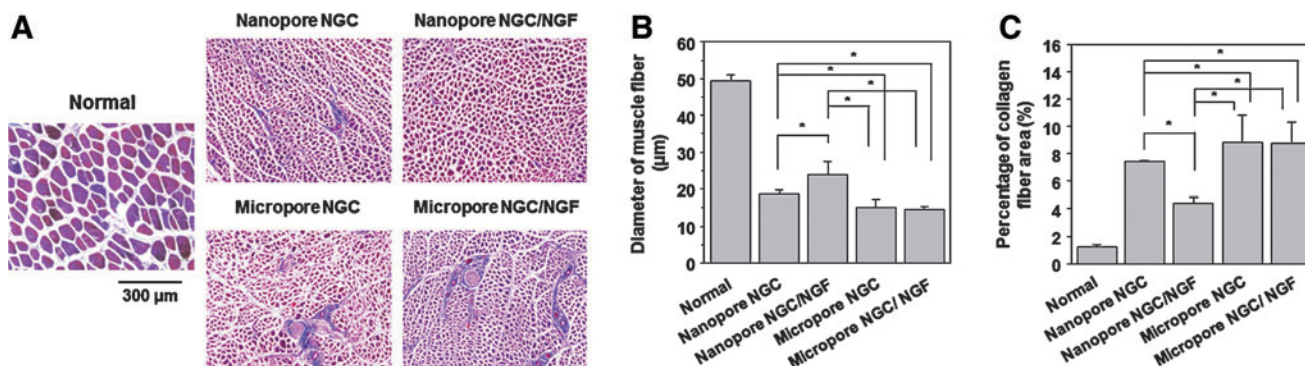


FIG. 11. (A) Light micrographs of gastrocnemius muscles (Masson's trichrome staining; $\times 100$), and their (B) diameter of muscle fibers and (C) percentage of collagen fiber area ($n=3$; $*p<0.05$). The Nanopore NGCs showed significantly faster recovery from muscle atrophy (thicker diameter of muscle fiber and smaller collagen fiber area) caused by the reinnervation of muscle than the Micropore NGCs. Color images available online at www.liebertpub.com/tec

Figures 5–10. Aebischer *et al.*³⁴ also suggested that the more intense host response on a rough surface than a smooth surface⁶³ leads to excessive synthesis of interleukin 1, which initiates the first cytokine to begin the inflammatory response, and the formation of connective stroma,⁶⁴ and, thus, the undesirable tissues prohibit nerve regeneration.

Conclusions

The NGCs with different surface pore structures (nanoporous inner surface vs. micro-porous inner surface) were fabricated by simply rolling the opposite side of asymmetrically porous PCL/F127 membranes, and the effect of the pore structure on peripheral nerve regeneration through the NGCs was investigated. In the animal study, the nerve fibers were found to be regenerated along the longitudinal direction through the NGC with a nano-porous inner surface (pore size, ~ 100 nm), while they were grown toward the porous wall of the NGC with a micro-porous inner surface (pore size, ~ 200 μ m). Based on the findings of this study, the NGC system with different surface pore structures but similar chemical/physical properties was determined to a good tool for investigating the effect of pores on nerve regeneration. More systematic experiments using NGCs with a range of pore sizes may be necessary for further elucidating the effect of surface pores in NGCs on nerve regeneration.

Acknowledgments

This work was supported by the Midcareer Research Program through a grant from the National Research Foundation (NRF) of Korea (No. 2011-0000244).

Disclosure Statement

No competing financial interests exist.

References

- Zhang, N., Yan, H., and Wen, X. Tissue-engineering approaches for axonal guidance. *Brain Res Brain Res Rev* **49**, 48, 2005.
- Seckel, B.R. Enhancement of peripheral nerve regeneration. *Muscle Nerve* **13**, 785, 1990.
- Schlosshauer, B., Müller, E., Schröder, B., Planck, H., and Müller, H.W. Rat Schwann cells in bioresorbable nerve guides to promote and accelerate axonal regeneration. *Brain Res* **963**, 321, 2003.
- Glück, T. Ueber neuroplastik aut dem wege der transplantation. *Arch Klin Chir* **25**, 606, 1880.
- Maquet, V., Martin, D., Malgrange, B., Franzen, R., Schoenen, J., Moonen, G., *et al.* Peripheral nerve regeneration using bioresorbable macroporous polylactide scaffolds. *J Biomed Mater Res* **52**, 639, 2000.
- Heath, C.A., and Rutkowski, G.E. The development of bioartificial nerve grafts for peripheral-nerve regeneration. *Trends Biotechnol* **16**, 163, 1998.
- Mackinnon, S.E., Dellon, A.L., Hudson, A.R., and Hunter, D.A. Chronic nerve compression - an experimental model in the rat. *Ann Plast Surg* **13**, 112, 1984.
- Ducker, T.B., and Hayes, G.J. Experimental improvements in the use of Silastic cuff for peripheral nerve repair. *J Neurosurg* **28**, 582, 1968.
- Keilhoff, G., Stang, F., Wolf, G., and Fansa, H. Biocompatibility of type I/III collagen matrix for peripheral nerve reconstruction. *Biomaterials* **24**, 2779, 2003.
- Fine, E.G., Valentini, R.F., Bellamkonda, R., and Aebischer, P. Improved nerve regeneration through piezoelectric vinylidene fluoride-trifluoroethylene copolymer guidance channels. *Biomaterials* **12**, 775, 1991.
- Fine, E.G., Decosterd, I., Papaliozos, M., Zurn, A.D., and Aebischer, P. GDNF and NGF released by synthetic guidance channels support sciatic nerve regeneration across a long gap. *Eur J Neurosci* **15**, 589, 2002.
- Danielson, N., Vahlsing, H.L., Pettman, B., Manthorpe, M., and Varon, S. Fibroblast growth factor effects on peripheral nerve regeneration in a silicone chamber model. *J Neurosci Res* **20**, 320, 1988.
- Park, S.C., Oh, S.H., and Lee, J.H. Fabrication and characterization of nerve growth factor-immobilized asymmetrically porous PDOCL/Pluronic F127 nerve guide conduit. *Tissue Eng Regen Med* **8**, 192, 2011.
- Kokai, L.E., Bourbeau, D., Weber, D., McAtee, J., and Marra, K.G. Sustained growth factor delivery promotes axonal regeneration in long gap peripheral nerve repair. *Tissue Eng* **17**, 1263, 2011.
- Guénard, V., Valentini, R.F., and Aebischer, P. Influence of surface texture of polymeric sheets on peripheral nerve

- regeneration in a two-component guidance system. *Biomaterials* **12**, 259, 1991.
16. Kim, Y., Haftel, V.K., Kumar, S., and Bellamkonda, R.V. The role of aligned polymer fiber-based constructs in the bridging of long peripheral nerve gaps. *Biomaterials* **29**, 3117, 2008.
 17. Hsu, S., and Ni, H.C. Fabrication of the microgrooved/microporous polylactide substrates as peripheral nerve conduits and *in vivo* evaluation. *Tissue Eng* **15**, 1381, 2009.
 18. Widmer, M.S., Gupta, P.K., Lu, L., Meszlenyi, R.K., Evans, G.R.D., Brandt, K., *et al.* Manufacture of porous biodegradable polymer conduits by an extrusion process for guided tissue regeneration. *Biomaterials* **19**, 1945, 1998.
 19. Hoppen, H.J., Leeslag, J.W., Pennings, A.J., van der Lei, B., and Robinson, P.H. Two-ply biodegradable nerve guide: basic aspects of design, construction and biological performance. *Biomaterials* **11**, 286, 1990.
 20. den Dunnen, W.F.A., Schakenraad, J.M., Zondervan, G.J., Pennings, A.J., van der Lei, B., and Robinson, P.H. A new PLLA/PCL copolymer for nerve regeneration. *J Mater Sci Mater Med* **4**, 521, 1993.
 21. Sundback, C., Hadlock, T., Cheney, M., and Vacanti, J. Manufacture of porous polymer nerve conduits by a novel low-pressure injection molding process. *Biomaterials* **24**, 819, 2003.
 22. Mackinnon, S.E., and Dellon, A.L. Clinical nerve reconstruction with a bioabsorbable polyglycolic acid tube. *Plast Reconstr Surg* **85**, 419, 1990.
 23. Bini, T.B., Gao, S., Xu, X., Wang, S., Ramakrishna, S., and Leong, K.W. Peripheral nerve regeneration by microbraided poly(L-lactide-co-glycolid) biodegradable polymer fibers. *J Biomed Mater Res* **68**, 286, 2004.
 24. Dalton, P.D., Flynn, L., and Shoichet, M.S. Manufacture of poly(2-hydroxyethyl methacrylate-co-methyl methacrylate) hydrogel tubes for use as nerve guidance channels. *Biomaterials* **23**, 3843, 2002.
 25. Kiyotani, T., Teramachi, M., Takimoto, Y., Nakamura, T., Shimizu, Y., and Endo, K. Nerve regeneration across a 25-mm gap bridged by a polyglycolic acid-collagen tube: a histological and electrophysiological evaluation of regenerated nerves. *Brain Res* **740**, 66, 1996.
 26. Evans, G.R.D., Brandt, K., Widmer, M.S., Lu, L., Meszlenyi, R.K., Gupta, P.K., *et al.* *In vivo* evaluation of poly(L-lactic acid) porous conduits for peripheral nerve regeneration. *Biomaterials* **20**, 1109, 1999.
 27. Chang, C.J., and Hsu, S.H. The effect of high outflow permeability in asymmetric poly(DL-lactic acid-co-glycolic acid) conduits for peripheral nerve regeneration. *Biomaterials* **27**, 1035, 2006.
 28. Chung, T.W., Yang, M.C., Tseng, C.C., Sheu, S.H., Wang, S.S., Huang, Y.Y., *et al.* Promoting regeneration of peripheral nerves *in-vivo* using new PCL-NGF/tirofiban nerve conduits. *Biomaterials* **32**, 734, 2011.
 29. Hsu, S.H., Chan, S.H., Chiang, C.M., Chen, C.C.C., and Jiang, C.F. Peripheral nerve regeneration using a microporous polylactic acid asymmetric conduit in a rabbit long-gap sciatic nerve transaction model. *Biomaterials* **32**, 3764, 2011.
 30. Zhu, Y., Wang, A., Patel, S., Kurpinski, K., Diao, E., Bao, X., *et al.* Engineering bi-layer nanofibrous conduits for peripheral nerve regeneration. *Tissue Eng* **17A**, 705, 2011.
 31. Oh, S.H., Kim, J.H., Song, K.S., Jeon, B.H., Yoon, J.H., Seo, T.B., *et al.* Peripheral nerve regeneration within an asymmetrically porous PLGA/pluronic F127 nerve guide conduit. *Biomaterials* **29**, 1601, 2008.
 32. Novack, C.R., Husby, J., Girado, J.M., Bassett, C.A.L., and Campbell, J.B. Neural regeneration across long gaps in mammalian peripheral nerves early morphological findings. *Anat Rec* **131**, 633, 1958.
 33. Young, B.L., Begovac, P., Stuart, D.G., and Goslow, G.E. An effective sleeving technique in nerve repair. *J Neurosci Methods* **10**, 51, 1985.
 34. Aebischer, P., Guénard, V., and Valentini, R.F. The morphology of regenerating peripheral nerves is modulated by surface microgeometry of polymeric guidance channels. *Brain Res* **531**, 211, 1990.
 35. Oh, S.H., Kim, T.H., Chun, S.Y., Park, E.K., and Lee, J.H. Enhanced guided bone regeneration by asymmetrically porous PCL/pluronic F127 membrane and ultrasound stimulation. *J Biomater Sci* 2011[Epub ahead of print]; DOI: 10.1163/092050611x589518).
 36. Oh, S.H., Kim, T.H., and Lee, J.H. Creating growth factor gradients in three dimensional porous matrix by centrifugation and surface immobilization. *Biomaterials* **32**, 8254, 2011.
 37. Smith, P.K., Mallia, A.K., and Hermanson, G.T. Colorimetric method for the assay of heparin content in immobilized heparin preparations. *Anal Biochem* **109**, 466, 1980.
 38. Shen, Y.H., Shoichet, M.S., and Radisic, M. Vascular endothelial growth factor immobilized in collagen scaffold promotes penetration and proliferation of endothelial cells. *Acta Biomater* **4**, 477, 2008.
 39. Oh, S.H., and Lee, J.H. Fabrication and characterization of hydrophilized porous PLGA nerve guide conduits by a modified immersion precipitation method, *J Biomed Mater Res* **80A**, 530, 2007.
 40. Broens, L., Altena, F.W., Smolders, C.A., and Koenhen, D.M. Asymmetric membrane structures as a result of phase separation phenomena. *Desalination* **32**, 33, 1980.
 41. Chung, Y.I., Tae, G., and Yuk, S.H. A facile method to prepare heparin-functionalized nanoparticles for controlled release of growth factors. *Biomaterials* **27**, 2621, 2006.
 42. Sun, W., Sun, C., Lin, H., Zhao, H., Wang, J., Ma, H., *et al.* The effect of collagen-binding NGF-beta on the promotion of sciatic nerve regeneration in a rat sciatic nerve crush injury model. *Biomaterials* **30**, 4649, 2009.
 43. Otto, D., Unsicker, K., and Grothe, C. Pharmacological effects of nerve growth factor and fibroblast growth factor applied to the transected sciatic nerve on neuron death in adult rat dorsal root ganglia, *Neurosci Lett* **83**, 156, 1987.
 44. Lyon, M., Rushton, G., and Gallagher, J.T. The interaction of the transforming growth factor-beta with heparin/heparan sulfate is isoform-specific. *J Biol Chem* **272**, 18000, 1997.
 45. Yoon, J.J., Chung, H.J., Lee, H.J., and Park, T.G. Heparin-immobilized biodegradable scaffolds for local and sustained release of angiogenic growth factor. *J Biomed Mater Res* **79A**, 934, 2006.
 46. Williams, L.R., Longo, F.M., Powell, H.C., Lundborg, G., and Varon, S. Spatial-temporal progress of peripheral nerve regeneration within a silicone chamber: parameters for a bioassay. *J Comp Neurol* **218**, 460, 1983.
 47. Chi, G.F., Kim, M., Kim, D.W., Jiang, M.H., Chung, E., and Son, Y. Repair of lateral hemisection lesion in spinal cord using Schwann cells differentiated from subcutaneous fat tissue delivered in fibrin plug. *Tissue Eng Regen Med* **8**, 262, 2011.
 48. Williams, L.R. Exogenous fibrin matrix precursors stimulate the temporal progress of nerve regeneration within a silicone chamber. *Neurochem Res* **12**, 851, 1987.

49. Liu, H.M. The role of extracellular-matrix in peripheral nerve regeneration: a wound chamber study. *Acta Neuropathol* **83**, 469, 1992.
50. Fawcett, J.W., and Keynes, R.J. The role of Schwann cells in the regeneration of peripheral nerve axons through muscle basal lamina grafts. *Annu Rev Neurosci* **13**, 43, 1990.
51. Daniloff, J.K. A novel assay for the *in vivo* study of Schwann cells. *Exp Neurol* **14**, 140, 1991.
52. Guenard, V., Kleitman, N., Morrissey, T.K., Bunge, R.P., and Aebischer, P. Syngenic Schwann cells derived from adult nerves seeded in semipermeable guidance channels enhance peripheral nerve regeneration. *J Neurosci* **12**, 3310, 1992.
53. Torigoe, K., Tanaka, H.F., Takahashi, A., Awaya, A., and Hashimoto, K. Basic behavior of migratory Schwann cells in peripheral nerve regeneration. *Exp Neurol* **137**, 301, 1996.
54. Williams, L.R., and Varon, S. Modification of fibrin matrix formation *in situ* enhances nerve regeneration in silicone chambers. *J Comp Neurol* **231**, 209, 1985.
55. Zhao, Q., Dahlin, L.B., Kanje, M., and Lundborg, G. Repair of the transected rat sciatic nerve: matrix formation within implanted silicone tubes. *Restor Neurol Neurosci* **5**, 197, 1993.
56. Scaravilli, F. The influence of distal environment on peripheral nerve regeneration across a gap. *J Neurocytol* **13**, 1027, 1984.
57. Valentini, R.F., Sabatini, A.M., Dario, P., and Aebischer, P. Polymer electrets guidance channels enhance peripheral nerve regeneration in mice. *Brain Res* **480**, 300, 1989.
58. Madison, R.D., da Silva, C., Dikkes, P., Sidman, R.L., and Chiu, T.H. Peripheral nerve regeneration with entubulation repair: comparison of biodegradable nerve guides versus polyethylene tubes and effects of a laminin-containing gel. *Exp Neurol* **95**, 378, 1987.
59. Miller, C., Shanks, H., Witt, A., Rutkowski, G., and Mallapragada, S. Oriented Schwann cell growth on micro-patterned biodegradable polymer substrates. *Biomaterials* **22**, 1263, 2001.
60. Manwaring, M.E., Walsh, J.F., and Tresco, P.A. Contact guidance induced organization of extracellular matrix. *Biomaterials* **25**, 3631, 2004.
61. Curtis, A., and Wilkinson, C. Topographical control of cells. *Biomaterials* **18**, 1573, 1997.
62. Jeong, J.Y., Kim, D.H., Park, S.H., Shin, J.W., Han, J.Y., Kang, Y.G., *et al.* Effects of PDMS surface patterns on differentiation and proliferation of MSCs under intermittent hydrostatic pressure. *Tissue Eng Regen Med* **7**, 283, 2010.
63. Taylor, S.R., and Gibbons, D.F. Effect of surface texture on the soft tissue response to polymer implants. *J Biomed Mater Res* **17**, 205, 1983.
64. Schmidt, J.A., Mizel, S.B., Cohen, D., and Green, I. Interleukin 1, a potential mediator of fibroblast proliferation. *J Immunol* **128**, 2177, 1982.

Address correspondence to:

Jin Ho Lee, PhD
Department of Advanced Materials
Hannam University
461-6 Jeonmin Dong, Yuseong Gu
Daejeon 305-811
South Korea

E-mail: jhlee@hnu.kr

Received: April 5, 2012

Accepted: August 3, 2012

Online Publication Date: September 12, 2012